

Article

Improved Dehydrogenation Properties of LiAlH₄ by Addition of Nanosized CoTiO₃

Nurul Amirah Ali , Muhammad Amirul Nawawi Ahmad , Muhammad Syarifuddin Yahya ,
Noratqah Sazelee  and Mohammad Ismail * 

Energy Storage Research Group, Faculty of Ocean Engineering Technology and Informatics, Universiti Malaysia Terengganu, Kuala Nerus 21030, Malaysia

* Correspondence: mohammadismail@umt.edu.my; Tel.: +60-9-6683487

Abstract: Despite the application of lithium aluminium hydride (LiAlH₄) being hindered by its sluggish desorption kinetics and unfavourable reversibility, LiAlH₄ has received special attention as a promising solid-state hydrogen storage material due to its hydrogen storage capacity (10.5 wt.%). In this work, investigated for the first time was the effect of the nanosized cobalt titanate (CoTiO₃) which was synthesised via a solid-state method on the desorption behaviour of LiAlH₄. Superior desorption behaviour of LiAlH₄ was attained with the presence of a CoTiO₃ additive. By means of the addition of 5, 10, 15 and 20 wt.% of CoTiO₃, the initial desorption temperature of LiAlH₄ for the first stage was reduced to around 115–120 °C and the second desorption stage was reduced to around 144–150 °C, much lower than for undoped LiAlH₄. The LiAlH₄-CoTiO₃ sample also presents outstanding desorption kinetics behaviour, desorbing hydrogen 30–35 times faster than undoped LiAlH₄. The LiAlH₄-CoTiO₃ sample could desorb 3.0–3.5 wt.% H₂ in 30 min, while the commercial and milled LiAlH₄ desorbs <0.1 wt.% H₂. The apparent activation energy of the LiAlH₄-CoTiO₃ sample based on the Kissinger analysis was decreased to 75.2 and 91.8 kJ/mol for the first and second desorption stage, respectively, lower by 28.0 and 24.9 kJ/mol than undoped LiAlH₄. The LiAlH₄-CoTiO₃ sample presents uniform and smaller particle size distribution compared to undoped LiAlH₄, which is irregular in shape with some agglomerations. The experimental results suggest that the CoTiO₃ additive promoted notable advancements in the desorption performance of LiAlH₄ through the in situ-formed AlTi and amorphous Co or Co-containing active species that were generated during the desorption process.

Keywords: lithium aluminium hydride; hydrogen storage; additives; cobalt titanate



Citation: Ali, N.A.; Ahmad, M.A.N.; Yahya, M.S.; Sazelee, N.; Ismail, M. Improved Dehydrogenation Properties of LiAlH₄ by Addition of Nanosized CoTiO₃. *Nanomaterials* **2022**, *12*, 3921.

<https://doi.org/10.3390/nano12213921>

Academic Editor: Jipeng Cheng

Received: 6 October 2022

Accepted: 4 November 2022

Published: 7 November 2022

Publisher's Note: MDPI stays neutral with regard to jurisdictional claims in published maps and institutional affiliations.



Copyright: © 2022 by the authors. Licensee MDPI, Basel, Switzerland. This article is an open access article distributed under the terms and conditions of the Creative Commons Attribution (CC BY) license (<https://creativecommons.org/licenses/by/4.0/>).

1. Introduction

Hydrogen is a clean and renewable energy carrier and has become the most preferred alternative to fossil fuels for the future energy system. The advancement of secure and effective solid-state hydrogen storage that operates at low temperature was the focus in developing practical hydrogen as a potential energy carrier, offering a high capacity of hydrogen and excellent reversibility. Recently, alanates have been considered favourable materials for solid-state hydrogen storage with high hydrogen capacity and operating at low temperatures compared to other hydrides [1,2]. Among the alanates, lithium aluminium hydride (LiAlH₄) has attracted considerable research interest. LiAlH₄ offers 10.5 wt.% hydrogen content [3]. Below 250 °C, LiAlH₄ is able to liberate a theoretical capacity of 7.9 wt.% H₂ [4,5]. Basically, LiAlH₄ decomposes to LiH and Al in a three-step reaction as follows [6,7]:



(occurs at 150–175 °C, releasing 5.3 wt.% H₂)



(occurs at 180–220 °C, releasing 2.6 wt.% H₂)



(occurs at >400 °C, releasing 2.6 wt.% H₂)

However, inadequate reversibility and unfavourable desorption kinetics of LiAlH₄ obstruct its progression to practical utilisation as a solid-state hydrogen storage medium [8]. Furthermore, the 2.6 wt.% H₂ in LiH as in Equation (3) is impracticable for applications owing to its high decomposition temperature (higher than 400 °C) [9]. To overcome these problems, several techniques have been introduced to accelerate the desorption behaviour of LiAlH₄—for example, the use of the nanoconfinement method and high energy ball milling [10–13], the usage of additives [14–17] and destabilisation with other hydrides [18–20].

The technique of high energy ball milling may exert a colossal effect on the behaviour of solid-state hydrogen storage materials by reducing the particle size that results in a larger surface area, hence shortening the distance of hydrogen diffusion [21,22]. The presence of additives, especially metal oxides, leads to a significant improvement, with a lower decomposition temperature and faster kinetic performance of LiAlH₄ due to enhanced catalytic support [23–26]. For instance, Li et al. [27] demonstrated satisfactory desorption behaviour of LiAlH₄ with the addition of NiCo₂O₄. The LiAlH₄-NiCo₂O₄ sample could release 4.95 wt.% H₂ at 130 °C in 150 min, while undoped LiAlH₄ only releases <1.0 wt.% H₂ within the same period. Then, Sulaiman et al. [28] showed that LiAlH₄ added with SrFe₁₂O₁₉ began to decompose at temperatures of 80 °C (first stage) and 130 °C (second stage), which are lower than undoped LiAlH₄. They also observed the formation of Fe, LiFeO₂, Sr and Sr-containing species during the heating process, which are advantageous in boosting the desorption properties of LiAlH₄. Furthermore, Li et al. [29] presented a study on the influence of CoFe₂O₄ on the desorption of LiAlH₄. Surprisingly, the performance of LiAlH₄ was significantly enhanced with rapid hydrogen desorption and low dehydrogenation activation energy. The LiAlH₄-CoFe₂O₄ sample could desorb 6.8 wt.% H₂ in 160 min, 6.1 wt.% higher than undoped LiAlH₄. Moreover, the activation energy of the LiAlH₄-CoFe₂O₄ composites decreased by 42.4 kJ/mol (first stage) and 86.1 kJ/mol (second stage) compared to pure LiAlH₄. The enhanced performance of the LiAlH₄-CoFe₂O₄ composite was attributed to the formation of Fe and Co species due to the reaction between LiAlH₄ and CoFe₂O₄. Then, another study revealed that the addition of TiO₂ could notably downshift the decomposition temperature of LiAlH₄ to 60 °C [30]. Desorption kinetics performance at 100 °C demonstrated that a TiO₂-doped LiAlH₄ composite could desorb 5.2 wt.% H₂ in 30 min, whereas the commercial LiAlH₄ desorbed only <0.2 wt.% H₂ in the same time but at a higher temperature (120 °C). The addition of TiO₂ offers significant enhancement of the performance of LiAlH₄ that may be ascribed to the introduction of a high density of defects on the surfaces of the TiO₂ particles throughout the ball milling process.

Inspired by the superior performance of the metal oxide additives, it is motivating to discover the consequence of another metal oxide on the desorption behaviour of LiAlH₄. The metal oxide additives may present outstanding performance compared to metal because of the bulk of oxides and the transition metal ions on the surface that may encounter different crystal fields due to the lack of ions at the surface of these oxides. This allows the electronic 3d state of the ions to be separated and is beneficial for the catalytic activity of transition metal oxides in the adsorption of gas molecules [31]. In this study, nanosized cobalt titanate (CoTiO₃) as an additive was added to LiAlH₄ by means of a ball milling process to ameliorate the desorption behaviour of LiAlH₄. Nanosized approaches are favourable in decreasing the materials' particle size and reducing the hydrogen diffusion distance, accelerating the rate of hydrogen diffusion and nucleation sites for the desorption process [32]. Moreover, it is believed that nanosized CoTiO₃ could provide a superior performance of LiAlH₄ with low hydrogen release temperature and faster kinetics. Herein, different amounts of CoTiO₃ were milled together with LiAlH₄ to examine the desorption

behaviour of LiAlH_4 as well as its kinetics behaviour. Moreover, the possible catalytic mechanism of the desorption process for this system has been discussed in depth.

2. Materials and Methods

Without any prior processing, LiAlH_4 (95% pure) from Sigma Aldrich was used. The nanosized CoTiO_3 was synthesised via the solid-state method, as explained in our previous work [33]. Then, various amounts of CoTiO_3 (5 wt.%, 10 wt.%, 15 wt.% and 20 wt.%) were doped with LiAlH_4 to study its influence on the desorption behaviour of LiAlH_4 . The composite was milled together at a speed of 400 rpm for one hour using a planetary ball mill (NQM-0.4).

A Sievert-type pressure-composition-temperature apparatus from the Advanced Materials Corporation was operated to carry out the hydrogen desorption kinetics experiment and the temperature-programmed desorption (TPD). The TPD test was carried out in a vacuum chamber and heated to 250 °C for the purpose of finding the initial desorption temperature. Experiments for the isothermal desorption tests were carried out at 90 °C and 1.0 atm H_2 pressure. Using a Mettler Toledo TGA/DSC 1, differential scanning calorimetry (DSC) measurements were carried out to analyse the thermal characteristics and determine the activation energy. For each characterisation, 6–8 mg of the sample was loaded in a crucible and heated to 300 °C with a flow of argon (50 mL/min) at several heating rates (15 °C/min, 20 °C/min, 25 °C/min and 30 °C/min).

The phase structure of the LiAlH_4 - CoTiO_3 sample after milling and after the desorption sample was examined using a Rigaku MiniFlex X-ray diffraction (XRD) system with $\text{Cu K}\alpha$ radiation. The sample was tested at a rate of 2.00°/min over diffraction angles of 20° to 80°. The sample's morphology and microstructure were then examined with a scanning electron microscope ((SEM; JEOL, Akishima, Tokyo, Japan) (JSM-6350LA)). The Fourier transform infrared (FTIR) spectrometer was tested in the range of 700 and 2000 cm^{-1} using IR Shimadzu Tracer-100.

3. Results and Discussions

The influence of CoTiO_3 on the initial desorption temperature of LiAlH_4 was characterised by the TPD experiment, as presented in Figure 1. By referring to the figure, the addition of CoTiO_3 results in superior desorption performance of LiAlH_4 . Commercial LiAlH_4 begins to release hydrogen at 145 °C (first stage) and 175 °C (second stage) releasing around 7.4 wt.% H_2 . After 1 h of milling, the temperature to release hydrogen was similar to the commercial LiAlH_4 , demonstrating that the milling process had a negligible influence on the desorption temperature of LiAlH_4 . Contrarily, by adding different amounts of CoTiO_3 (5, 10, 15 and 20 wt.%), the hydrogen release initiates at a much lower temperature than commercial and milled LiAlH_4 . The LiAlH_4 + 5 wt.% CoTiO_3 sample began to release hydrogen at 120 °C (first stage) and 150 °C (second stage), releasing 6.9 wt.% H_2 . Furthermore, increasing the amount of CoTiO_3 to 10 wt.% resulted in a decrease in hydrogen release temperature to 115 °C (first stage) and 145 °C (second stage), releasing 6.2 wt.% H_2 . Adding 15 wt.% of CoTiO_3 resulted in a similar temperature for hydrogen release as the LiAlH_4 + 10 wt.% CoTiO_3 sample. For the LiAlH_4 + 20 wt.% CoTiO_3 sample, hydrogen release occurs at 118 °C (first stage) and 144 °C (second stage), releasing 6.0 wt.% H_2 . The hydrogen release temperature for all of the CoTiO_3 -doped LiAlH_4 samples was much lower for than the undoped LiAlH_4 . Notably, with the amount of hydrogen released being slightly reducing compared to the undoped LiAlH_4 , the presence of CoTiO_3 provides positive contributions in lowering the temperature for the LiAlH_4 to release hydrogen. The amount of hydrogen released for all of the CoTiO_3 -doped LiAlH_4 samples was slightly reduced compared to undoped LiAlH_4 due to the deadweight of CoTiO_3 that does not hold any hydrogen [10,34].

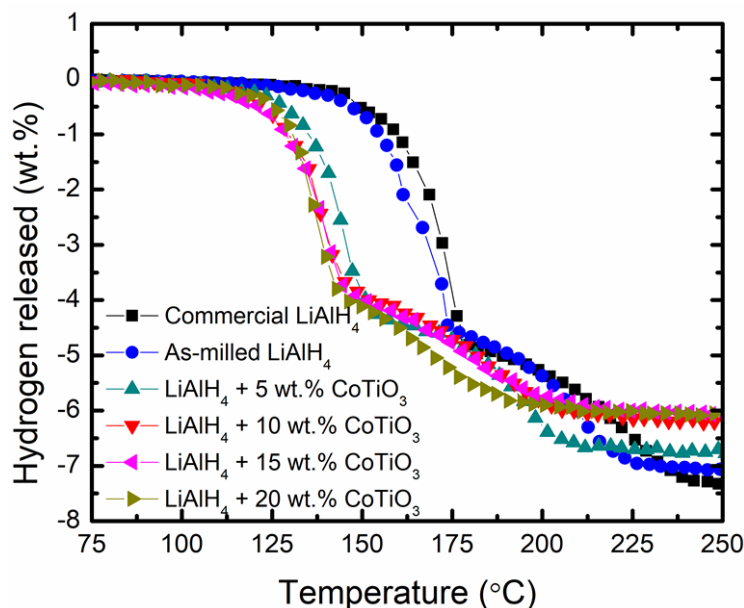


Figure 1. TPD profile of commercial LiAlH_4 , as-milled LiAlH_4 and $\text{LiAlH}_4 + x\text{CoTiO}_3$ ($x = 5, 10, 15$ and 20 wt.%).

Additionally, Figure 2 demonstrates the desorption kinetic performance of LiAlH_4 with and without CoTiO_3 at 90°C . As shown in Figure 2, the $\text{LiAlH}_4 + x\text{CoTiO}_3$ ($x = 5, 10, 15$ and 20 wt.%) releases a large amount of hydrogen in a short period of time. Within 30 min, the $\text{LiAlH}_4\text{-CoTiO}_3$ sample releases 3.0–3.5 wt.% H_2 . However, the undoped LiAlH_4 shows sluggish kinetics, with the ability to release only <0.1 wt.% H_2 within the same period. The addition of CoTiO_3 results in accelerated desorption kinetics which are 30–35 times faster than undoped LiAlH_4 . The rapid hydrogen release from the $\text{LiAlH}_4\text{-CoTiO}_3$ sample could be related to the creation of surface defects and active materials as a result of a reaction between LiAlH_4 and CoTiO_3 . Therefore, it can be concluded that the kinetic behaviour of LiAlH_4 can be enhanced by introducing CoTiO_3 . Considering the initial desorption temperature and the desorption kinetics performance, the $\text{LiAlH}_4 + 10$ wt.% CoTiO_3 sample is selected to further examine the effect of CoTiO_3 on the desorption behaviour of LiAlH_4 .

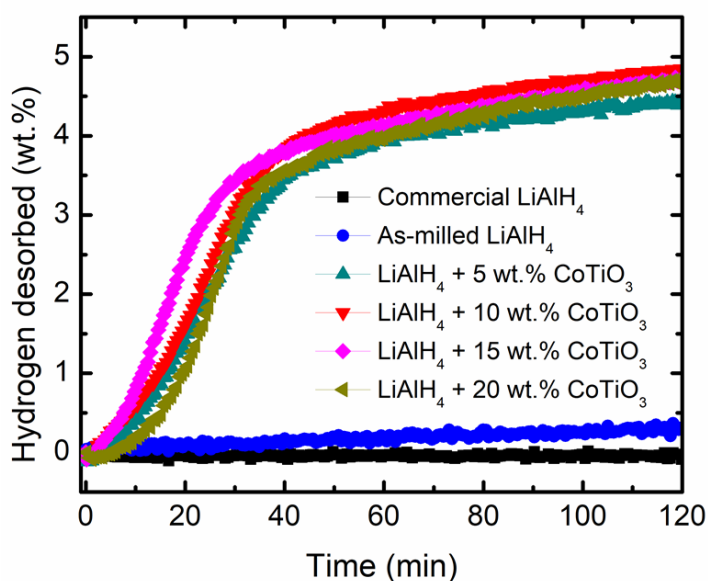


Figure 2. The desorption kinetic curve of commercial LiAlH_4 , as-milled LiAlH_4 and $\text{LiAlH}_4 + x\text{CoTiO}_3$ ($x = 5, 10, 15$ and 20 wt.%).

The effect of CoTiO_3 on the thermal behaviour of LiAlH_4 was characterised by DSC, as indicated in Figure 3. By referring to Figure 3, the thermal properties of as-milled LiAlH_4 consist of four peaks attributed to the two endothermic and two exothermic peaks. The first exothermic peak (140°C) was due to the interaction of hydroxyl impurities at the surface of LiAlH_4 , while the first endothermic peak (163°C) is attributed to the melting of LiAlH_4 . The second exothermic peak (175°C) is ascribed to the process of LiAlH_4 decomposing to Li_3AlH_6 and Al , while the second endothermic peak (230°C) relates to the process of Li_3AlH_6 decomposing to LiH and Al . Upon the addition of CoTiO_3 , the number of peaks was decreased to two, namely one endothermic peak and one exothermic peak, respectively, that occur at a lower temperature than for milled LiAlH_4 . The exothermic peak (LiAlH_4 decomposition) occurs at 105°C and the endothermic peak (Li_3AlH_6 decomposition) occurs at 196°C . Implying that the melt of LiAlH_4 is inhibited after the addition of the nanosized CoTiO_3 , the $\text{LiAlH}_4 + 10\text{ wt.}\% \text{CoTiO}_3$ sample begins to decompose prior to melting. These observations are consistent with the previous reports [35,36].

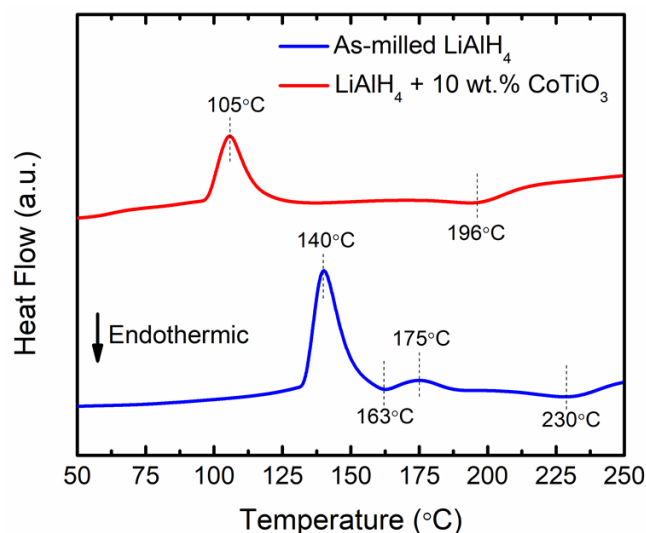


Figure 3. DSC profile of as-milled LiAlH_4 and $\text{LiAlH}_4 + 10\text{ wt.}\% \text{CoTiO}_3$ (heating rate: $15^\circ\text{C}/\text{min}$).

To scrutinise the impact of nanosized CoTiO_3 addition on the desorption activation energy of LiAlH_4 , the DSC measurement was performed at several heating rates. The DSC profiles of as-milled LiAlH_4 and $\text{LiAlH}_4 + 10\text{ wt.}\% \text{CoTiO}_3$ at several heating rates are shown in Figure 4. As depicted in the figure, the decomposition peak of $\text{LiAlH}_4 + 10\text{ wt.}\% \text{CoTiO}_3$ occurs at a lower temperature than that of undoped LiAlH_4 . The apparent activation energy (E_A) could be fitted from the DSC curve and calculated by Kissinger analysis as follows:

$$\ln[\beta/T_p^2] = -E_A/RT_p + A, \quad (4)$$

where β is the heating rate, T_p is the endothermic peak related to the decomposition temperature, E_A is the activation energy, R is the gas constant and A is a linear constant.

Then, the activation energy is determined based on the Kissinger plot of $\ln[\beta/T_p^2]$ versus $1000/T_p$, as in Figure 5. The activation energy of the undoped LiAlH_4 for the first and second desorption stage are 103.2 and 116.7 kJ/mol, respectively, based on the Kissinger plot. By adding nanosized CoTiO_3 , the activation energy of LiAlH_4 was notably decreased to 75.2 and 91.8 kJ/mol for the first and second desorption stage, respectively, being lowered by 27% for the first stage and 21% for the second stage compared to undoped LiAlH_4 . The reduced activation energy was in good agreement with the reduced decomposition temperature. From these results, it can be clearly seen that the introduction of CoTiO_3 as an additive remarkably reduced the activation energy of LiAlH_4 , demonstrating that CoTiO_3 has a favourable impact on the desorption behaviours of LiAlH_4 .

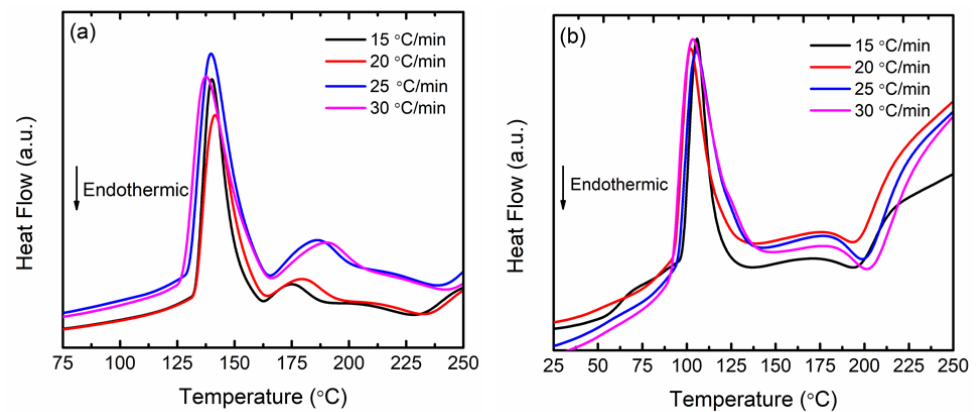


Figure 4. DSC profile of (a) as-milled LiAlH₄ and (b) LiAlH₄ + 10 wt.% CoTiO₃ at different heating rates.

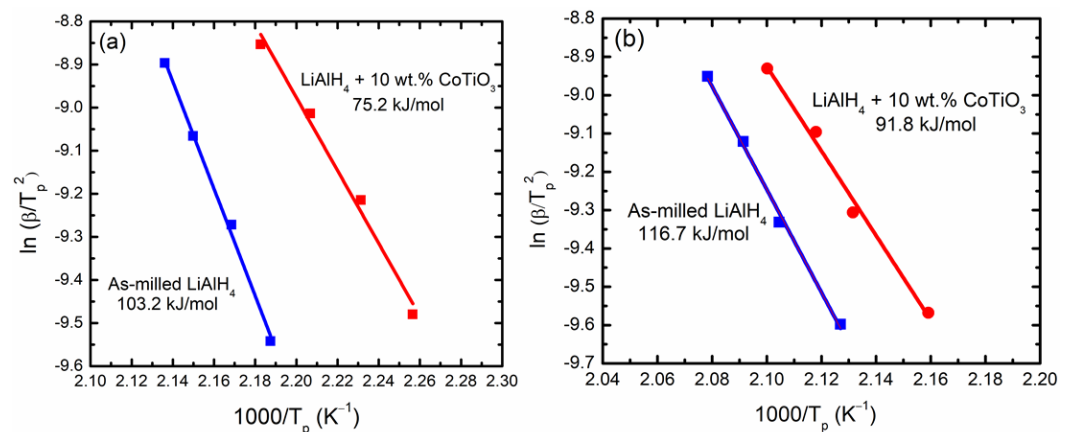


Figure 5. Kissinger plot of (a) first and (b) second desorption stage of as-milled LiAlH₄ and LiAlH₄ + 10 wt.% CoTiO₃.

Figure 6 displays the SEM micrograph of commercial LiAlH₄, as-milled LiAlH₄ and LiAlH₄ + 10 wt.% CoTiO₃ sample. By referring to Figure 6a, commercial LiAlH₄ consists of large uniform and blocky-shaped particles. After undergoing the milling process of one hour (Figure 6b), the blocky shape was broken into non-uniform smaller particles, but with some agglomerations. Meanwhile, after the addition of CoTiO₃, as shown in Figure 6c, the particle was transformed to a finer shape and size. The morphology of the composite sample (CoTiO₃-doped LiAlH₄) presents more uniform distributions with fewer agglomerations. The difference in morphology between the milled LiAlH₄ and LiAlH₄ + 10 wt.% CoTiO₃ sample may be due to the presence of an additive that acts as a lubricant and prevents the agglomerations of the sample. These superfine particles could facilitate the rapid hydrogen desorption of LiAlH₄ [32]. As reported previously, metal oxide-based additives have shown good lubricating performance [37,38]. This indicates that the addition of CoTiO₃ is favourable in constraining the agglomeration of the LiAlH₄ and results in a smaller and finer shape of the particle.

Figure 7 presents the particle distribution size of commercial LiAlH₄, as-milled LiAlH₄ and LiAlH₄ + 10 wt.% CoTiO₃ sample evaluated by the Image J software. The average particle size of the commercial LiAlH₄, as-milled LiAlH₄ and LiAlH₄ + 10 wt.% CoTiO₃ sample was calculated to be ~44, 0.5 and 0.3 μm, respectively. The morphological alteration and significant size reduction are responsible for the large surface defects and the expansion of grain boundaries across the composite's surface [39]. Resulting in more reactions for the nucleation sites and better diffusion channels of hydrogen being achieved with amplified grain boundaries that enhance the desorption behaviour of the LiAlH₄-CoTiO₃ sample with rapid desorption kinetics and lower activation energy, accelerating the rate of hydrogen diffusion [40], the reduction in particle size also results in a shorter hydrogen diffusion

path. Similarly, other findings also found that smaller and finer particle distributions demonstrated superior dehydriding performance of LiAlH_4 [36,41].

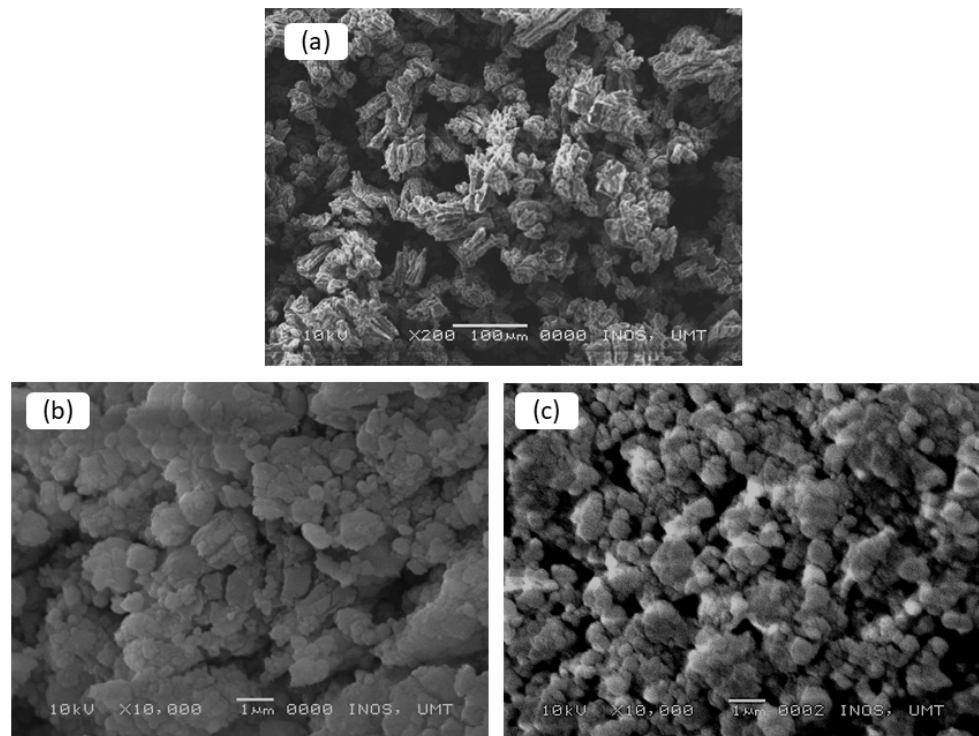


Figure 6. SEM images of (a) commercial LiAlH_4 , (b) as-milled LiAlH_4 and (c) LiAlH_4 + 10 wt.% CoTiO_3 sample.

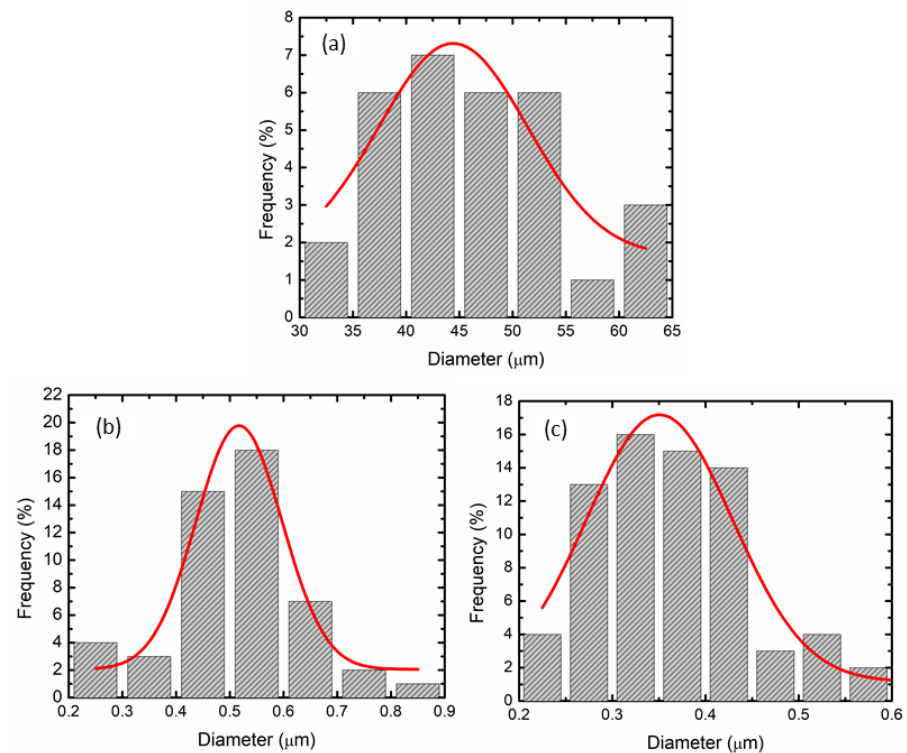


Figure 7. The particle size distribution of (a) commercial LiAlH_4 , (b) as-milled LiAlH_4 and (c) LiAlH_4 + 10 wt.% CoTiO_3 .

To discover the reaction mechanism during the milling process, XRD analysis was carried out as presented in Figure 8. Figure 8a shows the XRD peaks of commercial LiAlH_4 , and it appears that only peaks of LiAlH_4 were discovered, indicating the high purity of LiAlH_4 . For the milled sample (Figure 8b), similar to commercial LiAlH_4 , only peaks of LiAlH_4 were detected, suggesting that, similar to a previous report [42], LiAlH_4 maintains high stability throughout the milling process. Meanwhile, for the $\text{LiAlH}_4 + 10 \text{ wt.}\% \text{ CoTiO}_3$, as shown in Figure 8c, only LiAlH_4 peaks were visible, while the peaks of CoTiO_3 were not identified by the XRD, indicating that the amount of CoTiO_3 was too small to be detected by the XRD. This phenomenon was comparable to a prior work where several additives such as Ti_3C_2 and FeCl_2 were not detected by XRD [2,43].

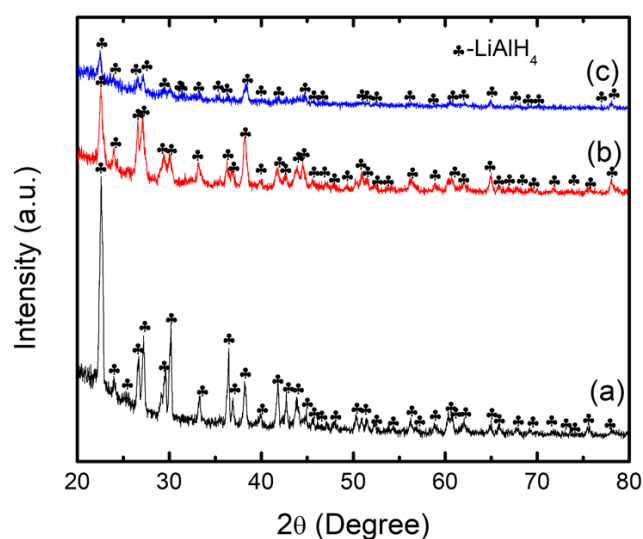


Figure 8. The XRD profile of (a) commercial LiAlH_4 , (b) as-milled LiAlH_4 and (c) $\text{LiAlH}_4 + 10 \text{ wt.}\% \text{ CoTiO}_3$.

Figure 9 depicts the FTIR spectra of commercial LiAlH_4 , as-milled LiAlH_4 and $\text{LiAlH}_4 + 10 \text{ wt.}\% \text{ CoTiO}_3$ sample. FTIR analysis was performed to determine the existence of Li_3AlH_6 after the milling process. All three samples exhibit two distinct region modes around $800\text{--}900 \text{ cm}^{-1}$, corresponding to the Li-Al-H bending mode, and $1600\text{--}1800 \text{ cm}^{-1}$, attributed to the Al-H stretching mode. However, for the $\text{LiAlH}_4 + 10 \text{ wt.}\% \text{ CoTiO}_3$ sample (Figure 9c), an extra absorbance peak around 1400 cm^{-1} was identified, indicating the presence of the Al-H stretching mode corresponding to the Li_3AlH_6 . This result proves that LiAlH_4 was slightly decomposed to Li_3AlH_6 during the milling process of LiAlH_4 and CoTiO_3 .

To explore the specific mechanism and catalytic activity of CoTiO_3 that contributed to the superior desorption behaviours of LiAlH_4 , the 10 wt.% and 20 wt.% CoTiO_3 -doped LiAlH_4 samples after desorption at $250 \text{ }^\circ\text{C}$ were analysed using XRD, as depicted in Figure 10. After the desorption process of the 10 wt.% CoTiO_3 -doped LiAlH_4 sample (Figure 10a), the main peaks detected are the dehydrogenated products of LiAlH_4 , which are LiH and Al, denoting that the complete desorption process of LiAlH_4 occurs. Moreover, the peaks of AlTi were also detected, indicating that there is a reaction between LiAlH_4 and CoTiO_3 . However, the peaks of Co or Co-containing species were not identified. The additional characterisation was carried out with 20 wt.% of CoTiO_3 (Figure 10b). Similarly, the main peaks of LiH and Al were observed with the additional peak of AlTi, and the fact that no peaks of Co or Co-containing species were identified after the desorption process may be due to the amorphous form of Co or Co-containing species.

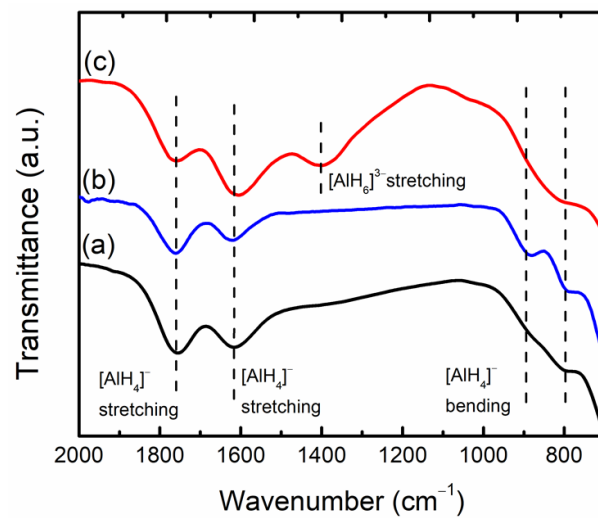


Figure 9. The FTIR profile of (a) commercial LiAlH_4 , (b) as-milled LiAlH_4 and (c) LiAlH_4 + 10 wt.% CoTiO_3 .

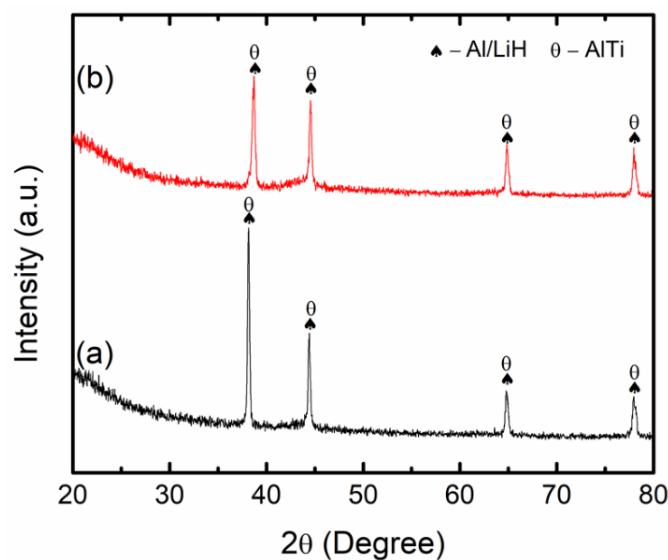


Figure 10. The XRD profile of (a) LiAlH_4 + 10 wt.% CoTiO_3 and (b) LiAlH_4 + 20 wt.% CoTiO_3 after desorption at 250 °C.

Referring to the results, it is noteworthy to state that the desorption behaviours of LiAlH_4 were improved due to the in situ formation of active species during the heating process. In this study, the formation of AlTi and Co or Co-containing species was believed to contribute to the enhanced desorption behaviours of LiAlH_4 . This phenomenon agrees with a previous study that also reported the formation of AlTi after the dehydrogenation process of LiAlH_4 [3,44]. The in situ formation of AlTi is beneficial in ameliorating the desorption behaviour of LiAlH_4 by catalysing the dehydrogenation through reaction in Equations (1) and (2). In addition, the study performed by Wohlwend et al. [45] revealed the superior performance of LiAlH_4 with the addition of Ti-based additives. The Ti atom reacts strongly with the LiAlH_4 surface and reduces the H binding energy. The reduction in binding energy may be a result of the correlation of the charge transfer change between Al and H that results in the accelerated kinetic performance of LiAlH_4 . It denotes that Co or Co-containing species also occupy a dominant role in improving the desorption behaviour of LiAlH_4 , even though the Co or Co-containing phase was not detected. For instance, a previous study discovered that the presence of Co_2O_3 exhibited a significant enhancement

in the desorption of LiAlH_4 compared to undoped LiAlH_4 [46]. Li et al. [29] also indicated that the formation of Co-containing species after the desorption process of LiAlH_4 provides a positive impact on the desorption behaviour of LiAlH_4 . Therefore, it is reasonable to infer that the formation of these active species contributes to the notable advancement of the desorption behaviour of LiAlH_4 . By shortening the length of diffusion of the reaction ions [29,41], these in situ-formed AlTi and Co or Co-containing species are responsible for boosting the desorption behaviour of LiAlH_4 by taking part as the active sites for the nucleation and creation of the dehydrogenation yield. However, further characterisation using X-ray photoelectron spectroscopy and transmission electron microscopy is needed to evaluate the actual impact and mechanism of the LiAlH_4 - CoTiO_3 system.

4. Conclusions

The introduction of nanosized CoTiO_3 that was synthesised via a solid-state method significantly ameliorates the desorption behaviour of LiAlH_4 . The LiAlH_4 - CoTiO_3 sample began to release hydrogen at around 115–120 °C and 144–150 °C for the first and second desorption stages, respectively, lower than for undoped LiAlH_4 . The addition of nanosized CoTiO_3 also results in accelerated desorption kinetics with the ability to desorb hydrogen 30–35 times faster than undoped LiAlH_4 . The rapid hydrogen desorption performance of LiAlH_4 when added with CoTiO_3 may be due to the lower activation energy of the LiAlH_4 - CoTiO_3 sample, which was calculated to be 75.2 kJ/mol (first stage) and 91.8 kJ/mol (second stage), reduced by 28.0 and 24.9 kJ/mol compared to undoped LiAlH_4 . The nanosized CoTiO_3 was also beneficial in the reduction of LiAlH_4 particle size during the milling process. Smaller particle size is favourable in reducing the hydrogen diffusion length, which then results in superior desorption performance. The enhanced desorption behaviour of LiAlH_4 was also due to the synergetic effect of the in situ formation of AlTi and Co or Co-containing species during the heating process of LiAlH_4 and CoTiO_3 . By reducing the initial desorption temperature and activation energy, the addition of nanosized CoTiO_3 remarkably ameliorates the desorption behaviour of LiAlH_4 , resulting in finer and smaller particles and accelerating the desorption kinetic behaviour. These findings shed light on the preparation of LiAlH_4 hydrogen storage systems for mobile applications.

Author Contributions: N.A.A., investigations, formal analysis and writing—original draft preparation; M.S.Y., writing—review and editing; N.S., writing—review and editing; M.A.N.A., writing—review and editing; M.I., supervision, writing—original draft preparation. All authors have read and agreed to the published version of the manuscript.

Funding: This study was supported by the Golden Goose Research Grant (GGRG) (VOT 55190) provided by Universiti Malaysia Terengganu.

Data Availability Statement: The data presented in this study are available on request from the corresponding author.

Acknowledgments: Universiti Malaysia Terengganu are fully acknowledged for supporting this study. N.A.A. and N.S. grateful for the scholarship provided by Universiti Malaysia Terengganu (SIPP and BUMT).

Conflicts of Interest: The authors declare no conflict of interest.

References

1. Tan, C.-Y.; Tsai, W.-T. Effects of Ni and Co-decorated MWCNTs addition on the dehydrogenation behavior and stability of LiAlH_4 . *Int. J. Hydrog. Energy* **2015**, *40*, 14064–14071. [[CrossRef](#)]
2. Xia, Y.; Zhang, H.; Sun, Y.; Sun, L.; Xu, F.; Sun, S.; Zhang, G.; Huang, P.; Du, Y.; Wang, J.; et al. Dehybridization effect in improved dehydrogenation of LiAlH_4 by doping with two-dimensional Ti_3C_2 . *Mater. Today Nano* **2019**, *8*, 100054. [[CrossRef](#)]
3. Zang, L.; Cai, J.; Zhao, L.; Gao, W.; Liu, J.; Wang, Y. Improved hydrogen storage properties of LiAlH_4 by mechanical milling with TiF_3 . *J. Alloys Compd.* **2015**, *647*, 756–762. [[CrossRef](#)]
4. Varin, R.; Zbronic, L. Fast and slow dehydrogenation of ball milled lithium alanate (LiAlH_4) catalyzed with manganese chloride (MnCl_2) as compared to nanometric nickel catalyst. *J. Alloys Compd.* **2011**, *509*, S736–S739. [[CrossRef](#)]

5. Humphries, T.D.; Birkmire, D.; McGrady, G.S.; Hauback, B.C.; Jensen, C.M. Regeneration of LiAlH₄ at sub-ambient temperatures studied by multinuclear NMR spectroscopy. *J. Alloys Compd.* **2017**, *723*, 1150–1154. [[CrossRef](#)]
6. Li, Z.; Liu, S.; Si, X.; Zhang, J.; Jiao, C.; Wang, S.; Liu, S.; Zou, Y.-J.; Sun, L.; Xu, F. Significantly improved dehydrogenation of LiAlH₄ destabilized by K₂TiF₆. *Int. J. Hydrog. Energy* **2012**, *37*, 3261–3267. [[CrossRef](#)]
7. Fu, J.; Röntzsch, L.; Schmidt, T.; Tegel, M.; Weißgärber, T.; Kieback, B. Comparative study on the dehydrogenation properties of TiCl₄-doped LiAlH₄ using different doping techniques. *Int. J. Hydrog. Energy* **2012**, *37*, 13387–13392. [[CrossRef](#)]
8. Li, L.; Wang, Y.; Jiao, L.; Yuan, H. Enhanced catalytic effects of Co@C additive on dehydrogenation properties of LiAlH₄. *J. Alloys Compd.* **2015**, *645*, S468–S471. [[CrossRef](#)]
9. Ali, N.A.; Sazelee, N.; Yahya, M.S.; Ismail, M. Influence of K₂NbF₇ catalyst on the desorption behavior of LiAlH₄. *Front. Chem.* **2020**, *8*, 457. [[CrossRef](#)]
10. Liu, S.-S.; Sun, L.-X.; Zhang, Y.; Xu, F.; Zhang, J.; Chu, H.-L.; Fan, M.-Q.; Zhang, T.; Song, X.-Y.; Grolier, J.P. Effect of ball milling time on the hydrogen storage properties of TiF₃-doped LiAlH₄. *Int. J. Hydrog. Energy* **2009**, *34*, 8079–8085. [[CrossRef](#)]
11. Fu, J.; Röntzsch, L.; Schmidt, T.; Weißgärber, T.; Kieback, B. Improved dehydrogenation properties of lithium alanate (LiAlH₄) doped by low energy grinding. *J. Alloys Compd.* **2012**, *525*, 73–77. [[CrossRef](#)]
12. Varin, R.A.; Parviz, R. The effects of the micrometric and nanometric iron (Fe) additives on the mechanical and thermal dehydrogenation of lithium alanate (LiAlH₄), its self-discharge at low temperatures and rehydrogenation. *Int. J. Hydrog. Energy* **2012**, *37*, 9088–9102. [[CrossRef](#)]
13. Wang, L.; Rawal, A.; Quadir, M.Z.; Aguey-Zinsou, K.-F. Nanoconfined lithium aluminium hydride (LiAlH₄) and hydrogen reversibility. *Int. J. Hydrog. Energy* **2017**, *42*, 14144–14153. [[CrossRef](#)]
14. Zhou, S.; Zou, J.; Zeng, X.; Ding, W. Effects of RE₃ (RE = Y, La, Ce) additives on dehydrogenation properties of LiAlH₄. *Int. J. Hydrog. Energy* **2014**, *39*, 11642–11650. [[CrossRef](#)]
15. Isobe, S.; Ikarashi, Y.; Yao, H.; Hino, S.; Wang, Y.; Hashimoto, N.; Ohnuki, S. Additive effects of TiCl₃ on dehydrogenation reaction of LiAlH₄. *Mater. Trans.* **2014**, *55*, 1138–1140. [[CrossRef](#)]
16. Sazelee, N.A.; Ismail, M. Recent advances in catalyst-enhanced LiAlH₄ for solid-state hydrogen storage: A review. *Int. J. Hydrog. Energy* **2021**, *46*, 9123–9141. [[CrossRef](#)]
17. Li, L.; Qiu, F.; Wang, Y.; Xu, Y.; An, C.; Liu, G.; Jiao, L.; Yuan, H. Enhanced hydrogen storage properties of TiN–LiAlH₄ composite. *Int. J. Hydrog. Energy* **2013**, *38*, 3695–3701. [[CrossRef](#)]
18. Sulaiman, N.N.; Ismail, M.; Timmiati, S.N.; Lim, K.L. Improved hydrogen storage performances of LiAlH₄+ Mg(BH₄)₂ composite with TiF₃ addition. *Int. J. Energy Res.* **2020**, *45*, 2882–2898. [[CrossRef](#)]
19. Meethom, S.; Kaewsuwan, D.; Chanlek, N.; Utke, O.; Utke, R. Enhanced hydrogen sorption of LiBH₄–LiAlH₄ by quenching dehydrogenation, ball milling, and doping with MWCNTs. *J. Phys. Chem. Solids* **2020**, *136*, 109202. [[CrossRef](#)]
20. Chen, G.; Zhang, Y.; Cheng, H.; Zhu, Y.; Li, L.; Lin, H. Effects of two-dimension MXene Ti₃C₂ on hydrogen storage performances of MgH₂–LiAlH₄ composite. *Chem. Phys.* **2019**, *522*, 178–187. [[CrossRef](#)]
21. Rattan Paul, D.; Sharma, A.; Panchal, P.; Chaudhary, S.; Patidar, D.; Nehra, S.P. Effect of ball milling and iron mixing on structural and morphological properties of magnesium for hydrogen storage application. *Mater. Today* **2021**, *42*, 1673–1677. [[CrossRef](#)]
22. Alsabawi, K.; Gray, E.M.; Webb, C.J. The effect of ball-milling gas environment on the sorption kinetics of MgH₂ with/without additives for hydrogen storage. *Int. J. Hydrog. Energy* **2019**, *44*, 2976–2980. [[CrossRef](#)]
23. Ali, N.; Idris, N.; Sazelee, N.; Yahya, M.; Yap, F.H.; Ismail, M. Catalytic effects of MgFe₂O₄ addition on the dehydrogenation properties of LiAlH₄. *Int. J. Hydrog. Energy* **2019**, *44*, 28227–28234. [[CrossRef](#)]
24. Sazelee, N.; Yahya, M.; Idris, N.; Din, M.M.; Ismail, M. Desorption properties of LiAlH₄ doped with LaFeO₃ catalyst. *Int. J. Hydrog. Energy* **2019**, *44*, 11953–11960. [[CrossRef](#)]
25. Rafi-ud-din; Xuanhui, Q.; Ping, L.; Zhang, L.; Ahmad, M. Hydrogen sorption improvement of LiAlH₄ catalyzed by Nb₂O₅ and Cr₂O₃ nanoparticles. *J. Phys. Chem. C* **2011**, *115*, 13088–13099. [[CrossRef](#)]
26. Liu, S.; Ma, Q.; Lü, H.; Zheng, X.; Feng, X.; Xiao, G.; Zheng, J. Study on hydrogen release capacity of LiAlH₄ doped with CeO₂. *Rare Metal Mat. Eng.* **2014**, *43*, 544–547. [[CrossRef](#)]
27. Li, L.; An, C.; Wang, Y.; Xu, Y.; Qiu, F.; Wang, Y.; Jiao, L.; Yuan, H. Enhancement of the H₂ desorption properties of LiAlH₄ doping with NiCo₂O₄ nanorods. *Int. J. Hydrog. Energy* **2014**, *39*, 4414–4420. [[CrossRef](#)]
28. Sulaiman, N.; Ismail, M. Catalytic effect of SrFe₁₂O₁₉ on the hydrogen storage properties of LiAlH₄. *Int. J. Hydrog. Energy* **2017**, *42*, 19126–19134. [[CrossRef](#)]
29. Li, Z.; Zhai, F.; Wan, Q.; Liu, Z.; Shan, J.; Li, P.; Volinsky, A.A.; Qu, X. Enhanced hydrogen storage properties of LiAlH₄ catalyzed by CoFe₂O₄ nanoparticles. *RSC Adv.* **2014**, *4*, 18989–18997. [[CrossRef](#)]
30. Ismail, M.; Zhao, Y.; Yu, X.B.; Nevirkovets, I.P.; Dou, S.X. Significantly improved dehydrogenation of LiAlH₄ catalysed with TiO₂ nanopowder. *Int. J. Hydrog. Energy* **2011**, *36*, 8327–8334. [[CrossRef](#)]
31. Barkhordarian, G.; Klassen, T.; Bormann, R. Catalytic mechanism of transition-metal compounds on Mg hydrogen sorption reaction. *J. Phys. Chem. B* **2006**, *110*, 11020–11024. [[CrossRef](#)] [[PubMed](#)]
32. Zhao, L.; Xu, F.; Zhang, C.; Wang, Z.; Ju, H.; Gao, X.; Zhang, X.; Sun, L.; Liu, Z. Enhanced hydrogen storage of alanates: Recent progress and future perspectives. *Prog. Nat. Sci. Mater.* **2021**, *31*, 165–179. [[CrossRef](#)]
33. Ali, N.A.; Yahya, M.S.; Sazelee, N.; Din, M.F.M.; Ismail, M. Influence of nanosized CoTiO₃ synthesized via a solid-state method on the hydrogen storage behavior of MgH₂. *Nanomaterials* **2022**, *12*, 3043. [[CrossRef](#)] [[PubMed](#)]

34. Xia, Y.; Wei, S.; Huang, Q.; Li, J.; Cen, X.; Zhang, H.; Chu, H.; Sun, L.; Xu, F.; Huang, P. Facile synthesis of NiCo₂O₄-anchored reduced graphene oxide nanocomposites as efficient additives for improving the dehydrogenation behavior of lithium alanate. *Inorg. Chem. Front.* **2020**, *7*, 1257–1272. [[CrossRef](#)]
35. Li, L.; Xu, Y.; Wang, Y.; Wang, Y.; Qiu, F.; An, C.; Jiao, L.; Yuan, H. NbN nanoparticles as additive for the high dehydrogenation properties of LiAlH₄. *Dalton Trans.* **2014**, *43*, 1806–1813. [[CrossRef](#)]
36. Cao, Z.; Ma, X.; Wang, H.; Ouyang, L. Catalytic effect of ScCl₃ on the dehydrogenation properties of LiAlH₄. *J. Alloys Compd.* **2018**, *762*, 73–79. [[CrossRef](#)]
37. Yap, F.H.; Ali, N.; Idris, N.; Ismail, M. Catalytic effect of MgFe₂O₄ on the hydrogen storage properties of Na₃AlH₆-LiBH₄ composite system. *Int. J. Hydrog. Energy* **2018**, *43*, 20882–20891. [[CrossRef](#)]
38. Aguey-Zinsou, K.-F.; Fernandez, J.A.; Klassen, T.; Bormann, R. Effect of Nb₂O₅ on MgH₂ properties during mechanical milling. *Int. J. Hydrog. Energy* **2007**, *32*, 2400–2407. [[CrossRef](#)]
39. Yuan, Z.; Sui, Y.; Zhai, T.; Yin, Y.; Luo, L.; Feng, D. Influence of CeO₂ nanoparticles on microstructure and hydrogen storage performance of Mg-Ni-Zn alloy. *Mater. Charact.* **2021**, *178*, 111248. [[CrossRef](#)]
40. Xu, X.; Zang, L.; Zhao, Y.; Zhao, Y.; Wang, Y.; Jiao, L. Hydrogen storage behavior of LiBH₄ improved by the confinement of hierarchical porous ZnO/ZnCo₂O₄ nanoparticles. *J. Power Sources* **2017**, *359*, 134–141. [[CrossRef](#)]
41. Ismail, M.; Sazelee, N.A.; Ali, N.A.; Suwarno, S. Catalytic effect of SrTiO₃ on the dehydrogenation properties of LiAlH₄. *J. Alloys Compd.* **2021**, *855*, 157475. [[CrossRef](#)]
42. Zhang, T.; Isobe, S.; Wang, Y.; Liu, C.; Hashimoto, N.; Takahashi, K. Enhanced hydrogen desorption properties of LiAlH₄ by doping lithium metatitanate. *Phys. Chem. Chem. Phys.* **2016**, *18*, 27623–27629. [[CrossRef](#)] [[PubMed](#)]
43. Cai, J.; Zang, L.; Zhao, L.; Liu, J.; Wang, Y. Dehydrogenation characteristics of LiAlH₄ improved by in situ formed catalysts. *J. Energy Chem.* **2016**, *25*, 868–873. [[CrossRef](#)]
44. Ismail, M.; Ali, N.A.; Sazelee, N.A.; Suwarno, S. Catalytic effect of Al₂TiO₅ on the dehydrogenation properties of LiAlH₄. *Int. J. Hydrog. Energy* **2022**, *47*, 31903–31910. [[CrossRef](#)]
45. Wohlfend, J.L.; Amama, P.B.; Shamberger, P.J.; Varshney, V.; Roy, A.K.; Fisher, T.S. Effects of titanium-containing additives on the dehydrogenation properties of LiAlH₄: A computational and experimental study. *J. Phys. Chem. C* **2012**, *116*, 22327–22335. [[CrossRef](#)]
46. Li, Z.; Li, P.; Wan, Q.; Zhai, F.; Liu, Z.; Zhao, K.; Wang, L.; Lü, S.; Zou, L.; Qu, X.; et al. Dehydrogenation improvement of LiAlH₄ catalyzed by Fe₂O₃ and Co₂O₃ nanoparticles. *J. Phys. Chem. C* **2013**, *117*, 18343–18352. [[CrossRef](#)]